INSIGHTS ON GA-ZEOLITE CATALYSTS: X-RAY POWDER DIFFRACTION AND ABSORPTION SPECTROSCOPY CHARACTERIZATION AT AMBIENT CONDITIONS

G. Beltrami[1*], T. Chenet[2], L. Pasti[2**], L. Gigli[3], S. Pollastri[4***] and A. Martucci[1]

[1]Dept. of Earth Sciences, University of Ferrara, Via Saragat, 1, I-44122 Ferrara, Italy.

[2]Dept. of Chemical and Pharmaceutical Sciences, University of Ferrara, Via Luigi Borsari, 43, I-44122 Ferrara, Italy.

[3]Elettra - Sincrotrone Trieste S.C.p.A. Strada Statale 14 34149 Basovizza, Trieste, Italy.

[4]CERIC-ERIC Strada Statale 14 34149 Basovizza, Trieste, Italy.

Keywords: Gallium substituted zeolite; XRPD; adsorption isotherm; XAS; Gallium location

ABSTRACT

Gallium substituted L, mordenite and ferrierite zeolites, obtained through wet impregnation, were characterized combining adsorption isotherms, X-ray powder diffraction (XRPD) and X-ray adsorption spectroscopy (XAS) to elucidate nature and structure of the Ga^{3+} sites of the materials. The saturation capacity of L was higher than those of mordenite and ferrierite. Rietveld refinements on saturated materials confirm the presence of Ga^{3+} within the zeolites pores system. Besides, the analysis of the structural features (*i.e.*, lightening of tetrahedral bond distances and narrowing of interthetraedral angles) suggest that small fractions of metal cation have been also incorporated in tetrahedral sites. This is corroborated by XAS analysis, which confirms the effective inclusion of gallium into the zeolites frameworks, thus indicating that the incorporation of Ga^{3+} from wet impregnation within the zeolite structures occurs in both framework and non-framework positions.

1. INTRODUCTION

Zeolite are crystalline microporous materials whose framework is build up by corner-sharing TO_4 tetrahedra, where T usually contain Si^{+4} or Al^{+3}. The insertion of other tetrahedral coordinated heteroatoms (*e.g.*, Fe, Ga, Ge, B, Ti, etc.) provides a means to modify their physicochemical properties as well as to increase their catalytic properties [1]. In addition, zeolite properties can be also modified by cation exchange process, in such a case, the type and localization of extraframework cations control and influence their selectivity and catalytic activity [2]. An interesting family of catalysts is that of Ga-loaded zeolites due to their excellent performances in isomerization, disproportionation and alkylation of aromatics and aromatization of alkanes and/or alkenes [3-6]. Gallium-containing zeolites have been widely investigated in the last decades and newest applications concerning the removal of NOx from gas streams of exhaust engine and the conversion of biomass into biofuels and bio-based chemicals have been proposed [5,7,8]. Ga-zeolite catalysts can be obtained through hydrothermal crystallization in presence of the suitable template agent or post synthesis treatments, such as galliation, recrystallization, wet impregnation, chemical vapor deposition (CVD) and ion exchange [5,9]. The ion exchange process is suitable to introduce gallium into both tetrahedral coordinated framework and interstitial non-framework positions. Besides, the precipitation on the external surface of the zeolite crystal of a separate gallium phase, depending on the pH value during the exchange process, in aqueous solution has to be foreseen. Substitution of Al^{+3} with Ga^{+3} cations [10] into framework positions is the main source of lattice charge defects, which give rise to Brønsted acidic Si-OH-Ga bridging hydroxyl group and, consequently, to modification of catalytic properties. To understand the precise nature and functioning of the active sites in working zeolites, incorporation of Ga^{3+} into the zeolite framework has been highlighted by means of solid-state NMR, EXAFS, in situ X-ray photoelectron spectroscopy, IR spectroscopy and DFT calculations. [11-17] Along with the segregate gallium phase, excess gallium not incorporated in tetrahedral sites is trapped within the zeolite pores system as substituent of metal cations, ammonium ions or protons. The presence of gallium cations in extraframework positions introduces Lewis acidity, which is also originated from oxo cations GaO+ in exchanged framework positions. Due to its size, gallium in framework positions is metastable; hence, the thermal treatment can cause the migration of Ga^{3+} to extraframework positions and its progressive aggregation in form of isolated, dimeric and polymeric species up to oxide nanoparticles [18-20]. This migration leads to the appearance of a different type of acid sites of Lewis nature [21]. As a consequence, Ga exchanged zeolites can possess both Brønsted and Lewis acid sites, working separately or in a synergistic way in acid catalysed reactions [22,23]. To our knowledge, in spite of the large number of both spectroscopic and or computational studies, very

few detailed structural investigations have been conducted so far to explore the gallium centres using X-ray diffraction methods. With this aim, in this work we intend to investigate the structural features of Ga-loaded zeolites in order to elucidate the nature of the gallium active sites combining X-ray powder diffraction (XRPD), X-ray absorption spectroscopy (XAS) and adsorption study.

Among zeolites, gallium modified L (L), mordenite (MOR) and ferrierite (FER), have been employed as catalysts [24]. Consequently, these large and medium pore materials were selected in this work to: 1) investigate the adsorptive properties of hydrophobic synthetic zeolites; 2) characterize zeolite structure at ambient conditions, 3) locate and quantify Ga^{+3} cations in framework and non-framework positions, 4) determine the presence of water molecules completing the extraframework Ga^{+3} coordination, 5) determine unit cell dimensions as well as host-guest interactions by the analysis of bond length distances. All these information are essential not only for their characterization but also for their industrial applications.

2. MATERIALS AND METHODS

2.1 Zeolites

The synthetic zeolite L sample (HSZ-500KOA code) was purchased by Tosoh Corporation in the K form, with a SiO_2/Al_2O_3 (SAR) ratio of 6.1, an Na_2O content of 0.25 wt % and a surface area of about 290 m^2/g. MOR (CBV10A code) and FER (CP914C code) samples were supplied by Zeolyst International in Na^+ and ammonium forms, respectively. The first is characterized by a SAR equal to 13, a Na_2O content of 6.5 wt % and a surface area of 425 m^2/g, whereas the second by a SAR equal to 20, Na_2O content lower than 0.05 wt % and surface area of 400 m^2g^{-1}.

2.2 Cation exchange

As-received L and MOR zeolites were exchanged with ammonium by the following procedure: 1 g of zeolite was stirred in 200 mL of 0.5 M solution of ammonium nitrate (>99%, Sigma Aldrich) in MilliQ water at 343 K for 24 h. The suspension was then filtered, by using a Nylon filer 0.22 μm (Sigma Aldrich) at room temperature and rinsed with 300 mL of MilliQ water. This procedure was repeated twice. The ammonium form of L and MOR and the as-received FER were heated in a furnace for five hours at ~ 600 °C in order to obtain the calcined-form.

3. EXPERIMENTAL TECHNIQUES

3.1 Wet impregnation

Cation exchange capacity was determined by using aqueous solutions of gallium nitrate ($Ga(NO_3)_3 \cdot xH_20$, Aldrich 99.9%) at different initial concentrations (5, 10, 20, 50, 70, 100, 150 and

200 mg L^{-1}), placed in contact with zeolites (L, FER and MOR) with a solid/liquid ratio of 1:1 (mg/mL). The suspensions were kept at 343 K under stirring during the contact time at pH 4.3, the pH was monitored during the contact and variation of 0.3 pH unit occur from the beginning to the end of the contact. All batch experiments were carried out in duplicate. The concentrations of Ga^{3+} in the solutions after the contact with zeolites and in the reference solutions obtained by keeping solutions in the same conditions of the adsorption experiments but without the addition of zeolites, were quantified by ICP-OES (Perkin-Elmer Optima 3100 XL) (axial view) equipped with a solid-state charge-coupled device detector (CCD), a peristaltic pump and a low-flow GemCone nebulizer coupled to a cyclonic spray chamber. Background correction was carried out using a two-points method. Analytical line 294.364 nm was selected for quantitative determination. The amount of exchanged cations at equilibrium, qe (mg g−1), was calculated from the mass balance equation, Eq. (1):

$$q_e = \frac{(C_i - C_e)\,V}{M} \quad (1)$$

where Ci and Ce (mg L^{-1}) are the liquid-phase concentrations of Ga in the reference solution and at equilibrium respectively; V (L) is the volume of the solution and M (g) is the mass of dry zeolite used. Samples of saturated zeolite exchanged with Ga were used for structural and spectroscopic investigations. Calcined Mordenite, Ferrierite and L zeolites (0.5 g) were suspended with stirring in 500 ml of an aqueous solution of gallium nitrate ($Ga(NO_3)_3 \cdot xH_20$, Aldrich 99.9%) at pH 4.2, 343 K for 24 h. The zeolite was recovered by filtration, washed with 200 mL of MilliQ water and dried in oven at 383 K overnight.

3.2 X-ray powder diffraction and Rietveld refinements

Powder patterns of the Ga-exchanged zeolites, here after called Ga-L Ga-MOR and Ga-FER were collected on a Bruker D8 Advance diffractometer equipped with a Si/Li solid state detector (Sol-X). Measurements were performed at Room Temperature, using the Cu$K\alpha 1,\alpha 2$ wavelength, in a 3-100 ° 2θ range. Full profile Rietveld refinements were performed through the GSAS software [25] and the EXPGUI graphical interface [26]. Refinements were performed using the hexagonal *P*6/*mmm* and the orthorhombic *Cmcm* and *Immm* space groups for Ga-L, Ga-MOR and Ga-FER systems, respectively. Details on the refined parameters are reported in Table 1 and below:

Ga-L. Peak profiles were modelled through the Pseudo-Voigt function with 0.1 % cut-off peak intensity. The profile function selected was the number 2 and the coefficients refined were: Gaussian θ-indipendent *GW*, Lorentian $\cos\theta^{-1}$ and $\tan\theta$-dependent *LX* and *LY* terms, peak

asymmetry and ptec parameters. The empirical background was fitted through the Chebyschev polynomial function and 18 coefficients.

Ga-MOR. Peak profiles were modelled through the Pseudo-Voigt function with 0.5 % cut-off peak intensity. The profile function selected was the number 2 and the coefficients refined were: Gaussian θ-indipendent *GW*, $\tan^2\theta$-dependent *GU*, $\tan\theta$-dependent *GV* and Lorentian $\cos\theta^{-1}$ dependent *LX* terms, peak asymmetry and *ptec* parameters. The empirical background was fitted through the Chebyschev polynomial function and 26 coefficients.

Ga-FER. Peak profiles were modelled through the Pseudo-Voigt function with 0.1 % cut-off peak intensity. The profile function selected was the number 2 and the coefficients refined were: Gaussian θ-indipendent *GW*, Lorentian $\cos\theta^{-1}$ and $\tan\theta$-dependent *LX* and *LY* terms, peak asymmetry parameter, *ptec* and *stec*. The empirical background was fitted through the Chebyschev polynomial function and 15 coefficients.

Scale factor and 2theta zero shift were also accurately refined for all the systems. Besides, in all the structural refinements soft constraints were initially imposed on tetrahedral distances (σ=0.04Å) and completely removed in the last refinement cycles. Whereas, atomic coordinates, site occupancies and isotropic atomic displacement parameters (UISO) were refined, constraining equivalent UISO for framework oxygen atoms of each system. Framework and extraframework fractional coordinates of Ga-L, Ga-MOR and Ga-FER systems are reported in Table SI1, Table SI2 and Table SI3, respectively.

3.3 X-ray Absorption Spectroscopy

Ga K-edge XAS spectra were collected at the XAFS beamline (ELETTRA, Trieste, Italy) [27] in transmission mode using fixed exit double crystal Si(111) monochromator. For all the samples, energy calibration was accomplished by collecting simultaneously a reference spectrum of a GaAs pellet placed in a second experimental chamber after the sample and after the I1 ionization chamber, with the position of the first inflection point taken at 10369.0 eV. All spectra were collected at room temperature and in vacuum conditions, with a variable energy step as a function of the energy: Large step (5 eV) in the first 200 eV of the spectrum, smaller step (0.2 eV) in the XANES region and a k-constant step of 0.03 $Å^{-1}$ (up to 1.8 eV) in the EXAFS region.

For each sample, 4 spectra have been collected and merged in order to increase the signal to noise ratio; merged spectra were then normalized with respect to the high-energy side of the curve and EXAFS signals have been extracted using the Athena software [28]. The extracted EXAFS signals were then Fourier transformed using a Hanning window in the k range 3 – 15 $Å^{-1}$ and quantitative analysis were carried out using the Artemis software (Demeter 0.9.25 package) [28,29].

Structural model for the calculation of the theoretical paths were retrieved by Rietveld refinements of the XRPD data of Ga-FER, Ga-MOR, Ga-L. Along with the samples, the compound $Ga(NO_3)_3 \cdot xH_2O$ used for the sample preparation was also measured as reference for octahedral coordinated gallium.

4. RESULTS AND DISCUSSION

4.1 Adsorption of Gallium on calcined zeolites

The gallium exchanged zeolites were obtained by wet impregnation by placing in contact aqueous solution of gallium nitrate with zeolites. During this process, the solution pH can affect the adoption, since in very acidic media (pH < 2) the stability of zeolite diminished and dissolution phenomena occurs with change in crystallinity and in composition (dealumination) of the adsorbent material [30]. On the other hand, Gallium undergoes hydrolysis and polymerization in aqueous solution, with increasing pH. Starting from pH > 2, a progressive formation of hydroxylated monomeric specie occurs and at slightly acid pH polymeric polycations are the dominant species. Therefore, a compromise pH value equal to 4 was selected for the experiments. The total quantity of gallium adsorbed from the solution at different concentrations were evaluated by atomic spectroscopy. In Fig.1 (a, b and c) the adsorption isotherms are reported, it can be seen that all the three zeolites show an L-Type isotherm, and zeolite L is characterized by a higher saturation capacity. The data were fitted by Langmuir and Tòth isotherm models given respectively by Eqs. (2) and (3):

$$q_e = \frac{q_s K_L c_e}{1 + b c_e} \tag{2}$$

$$q_e = \frac{q_s K_T c_e}{(1 + (b c_e)^v)^{1/v}} \tag{3}$$

where, q_s is the saturation capacity and K_L and $K_T$the affinity constant for the Langmuir and the Tóth models, respectively, in eq. 3 v represent the heterogeneity parameter. The fitting results are reported in Table 2, the values in parenthesis indicate the confidence limits at 95% of probability. As can be seen from the coefficient of determination listed in this table both the Langmuir and the Tóth models fit quite well the experimental data. In particular, for both L and FER, the heterogeneity parameter v appearing in the Tóth isotherm (see Table 2) is not significantly different from 1 and for v =1, the Tóth isotherm corresponds to the Langmuir one. On the contrary, for MOR a v value lower than 1 was found. The

heterogeneity parameter is related to the width of the energy distribution function, and lower value correspond to larger distribution and, therefore, to energetically heterogeneous sites on the surface. From the adsorption data therefore it seems that the adsorption onto MOR could involve sites of different energies. However, it should be mentioned that Langmuir isotherm has also been employed to describe the adsorption on multiple sites [31], in such cases it is supposed that their interactions energies are similar and they can be averaged to give a single averaged energy for all the sites. To gain more information on the involved site a structural investigation on the Ga-exchanged zeolites were carried out.

4.2 X-ray powder diffraction results

4.2.1 Ga-L system

Zeolite L (ideal formula $K_6Na_3Al_9Si_{27}O_{72}•21H_2O$, framework-type LTL) is a large pore material whose framework is built from columns of cancrinite cages stacked with double six membered rings (D6R) along the c axis [32]. The 4-rings in these columns are cross-linked to form continuous 12-ring channels along the *c*-direction with a maximum diameter of 12.6 Å [33]. The Ga-L crystal structure was refined in the *P*6/*mmm* space group, starting from the atomic coordinates reported by Barrer and Villiger, H. (1969) [33]. The refined Ga-L lattice parameters are the following: a=b=18.2177(24) Å, c= 7.5538(15) Å and V=2171.1(6) $Å^3$. According to Newsam [34] the framework bond distances confirm the not random distribution of Al (and/or Ga) in the tetrahedral sites (Table SI4). The T1-O bond lengths range from 1.630(4) and 1.668(3) Å (mean distance of 1.650 Å); whereas the T2-O ranges from 1.639(6), Å and 1.846(1) Å (mean distance 1.722 Å). Compared with the mean <T-O> bond lengths refined for the L-LTL precursor (<T1-O>=1.640 Å and <T2-O>=1.654 Å, *in preparation*), a lightening of both tetrahedral distances is observed. This result suggests the incorporation of gallium in both tetrahedral sites and a Ga-enrichment in the T2 one due to the longer average <T2-O> bond length. From the structural point of view, worth noting are the very narrow T-O-T angles centred on the O1 and O5 framework oxygen atoms (T1-O1-T1=112.6(5) and T2-O5-T2=115.4(3) °), even if they are not the narrowest found in zeolites [35-38] (Table SI4). The difference Fourier map generated using the GSAS package [25,26] highlights the presence of six extraframework sites which were distributed among K^+ and Ga^{+3} cations, and water molecules (Fig.2). The not-exchanged K^+ was localised at the centre of the 6MR (corresponding to the KB site in the L-LTL zeolite [33], within the cancrinite cage. Two extraframework sites were assigned to Ga^{+3} ions (*i.e.*, labelled Ga1 and Ga2, respectively) and were located not far from the centre of the 8MR (Ga1) and close to the edge of the12MR channel (Ga2), respectively. The remaining three partially occupied sites were all positioned within the 12MR channel and were attributed to H_2O molecules (*i.e.*, W1, W2 and W3 sites, respectively). K^+ is six-fold coordinated to

six framework oxygens, as suggested by the K1-O3=2.92[x6] Å distance. Ga1 is six-fold coordinated to O4 and O6 framework oxygen atoms (Ga1-O4= 2.85[x4] Å and Ga1-O6=2.21[x2] Å). The refined bond distances (Ga2-W1=2.67[x2] Å, Ga2-W2= 2.23[x2] Å and Ga2-W3=2.56[x4] Å) and occupancies of W1, W2 and/or W3 water molecules indicate that Ga2 is four (with W1 and W2, or only W3) or six-fold coordinated (with W1 or W2 and W3) to water. Indeed, bond distances suggest also the presence of short W1-W3-W3 water oligomers developing along the [*001*] direction, as testified by the W1-W3=2.26 and W3-W3= 2.98 Å distances. On the whole, Rietveld refinement reveals the occurrence of ~ 14 water molecules, 2 K^+ and 2.57 atoms of Ga^{+3} per unit cell, respectively. The K and Ga values were consistently lower than the theoretical concentration, which can be calculated on the basis of the aluminium content of the L precursor. This discrepancy cannot be attributed to an underestimation of the cations sites found in our refinements, neither to an incomplete NH_4^+ ion exchange or dehydroxylation and/or dealumination during calcination, as well as residual NH_4^+ after calcination. Moreover, difference Fourier (DF) map does not show any indication of extraframework sites, attributable to NH_4^+ groups. The hypothesis of extraframework Al atoms is also disregarded by the DF synthesis that does not show any maximum that can be interpreted as oxygen atoms coordinated to Al^{+3}. We suggested that the lattice charge defects give rise to Brønsted acidic Si-OH-Ga bridging hydroxyl group, whose occurrence is confirmed by the lengthening of the T-O distance after gallium incorporation. Recently, Beltrami et al. [personal communication] demonstrated the presence of Brønsted acid sites through neutron powder diffraction on the acidic form of zeolite L. The first site (D1) was located on the framework oxygen O5, not far from the centre of the 8-ring of the cancrinite cage. The second (D2 site) on the framework oxygen O1, heading towards the centre of the 12 MR channel. On the whole, 7.6 Brønsted sites were recognized, in consistence with the tetrahedral aluminium content determined starting from the Si/Al ratio. In our refinement, the T-O distances involving the O5 and O1 framework oxygens were always among the largest of the tetrahedra (Table SI4). At the same time, the attractive force of Brønsted acid sites could reasonably responsible of the very narrow T-O-T angles centred on the O1 and O5 framework oxygen atoms (T1-O1-T1=112.7(5) and T2-O5-T2=115.4(3)°).

As reported by Fricke et al. (2000) [5], the excess of gallium determines the formation of a segregate phase coexisting with the main zeolitic one. In this case, a phase of gallium hydroxide (GaO(OH)) was recognized through the qualitative analysis, which highlights the presence of some extra peaks (*i.e.*, [*101*], [*200*] and [*201*] *hkl* reflections at the 21.41 and 18.06 and 26.68 ° 2θ angles, respectively) not attributable to the L zeolite (Fig.3). The semi-quantitative analysis reveals the presence of 83 and 17 wt % of L zeolite and GaO(OH), respectively.

4.2.2 Ga-MOR system

Mordenite (ideal formula $[Na^{+}_{8}][Al_8Si_{40}O_{96}]\bullet 24H_2O$, framework type MOR) is a medium pore zeolite characterized by a monodimensional channel system, which consists of 12-membered rings running parallel to the [*001*] direction interconnected along the [*010*] direction through 8MR side pockets [32]. The crystal structure of the gallium-exchanged mordenite was refined using the topological orthorhombic *Cmcm* symmetry starting from the structural model of Alberti et al. (1986) [39]. After the Ga-exchange, lattice parameters highlight a slight reduction of the unit cell volume (Ga-MOR=2766.35(25) $Å^3$, Na-MOR=2781.58(25) $Å^3$) compared to the ones of the starting Na-MOR sample, due to the decrease of *b* and *c* parameters (Ga-MOR: *b*=20.3510(9) Å, *c*=7.4940(4) Å; Na-MOR: *b*=20.4447(10) Å, *c*= 7.5152(4) Å). On the contrary, along *a* direction, a small increase is observed (18.1387(9) and 18.1038(10) for Ga-MOR and Na-MOR, respectively). The comparison of the mean tetrahedral distances between the exchanged one (<T1-O>=1.662 Å, <T2-O>=1.654 Å, <T3-O>=1.658 Å, <T4-O>=1.657 Å) and the Na-form (<T1-O>=1.654 Å, <T2-O>=1.650 Å, <T3-O>=1.657 Å, <T4-O>=1.656 Å) does not show any indications about a preferential siting of gallium in framework position. On the contrary, intertetrahedral angles of the Ga-MOR are narrower than those of the starting material. Among them, noteworthy is the shrinkage of the T3-O9-T3 angle, which moves from 165.5° in the Na-MOR to 151.9° in the Ga-MOR (Table SI5). The analysis of the difference Fourier map allows to detect the presence of extraframework sites assigned to residual Na^+ cation, Ga^{+3} and water molecules, respectively (Fig.4). Not exchanged Na^+ (labelled Na2) is located within the 8MR in a six-fold coordination with O1 (Na2-O1=3.06 Å [x4]) and O6 (Na2-O6=3.01 Å [x2]) framework oxygen atoms. Gallium site (labelled Ga1) is positioned within the 12MR channel, along with all the three sites attributed to water molecules (W1, W2 and W3), which have a fundamental role in the completion of the gallium cation coordination. In this case, gallium is five-fold coordinated, as testified by the following bond distances: Ga1-W1=2.10 Å, Ga1-W2=2.09 Å [x2] and Ga1-W3=2.00 Å [x2]. Furthermore, W2 and W3 show to be hydrogen bonded each other (W2-W3=2.56 Å [x4]), thus forming short W2-W3 water oligomers running along the 12MR. No further residual electron density, attributable to NH_4^+ groups, were detected through the DF map, thus indicating that all the ammonium content has been substituted by Ga^{+3} and that the extraframework gallium quantified is the maximum exchangeable for our mordenite. Concerning the amount of extraframework content, refined occupancies indicate the presence of 2 and 1.16 a.u.c of Na^+ and Ga^{+3} cations, respectively, along with 13 water molecules per unit cell. Na^+ and Ga^{+3} values obtained are lower than the theoretical concentration, hence also in this case the presence of Brønsted acidic Si-OH-Ga bridging hydroxyl group has to be supposed to counterbalance the framework charge defect. Martucci et al. (2000) [40] reports that the

position of Brønsted acid sites does not strictly depends on the nature of the zeolite (natural or synthetic) and on its Si/Al ratio. Indeed, in all the three samples considered in that work (with Si/Al ratio equal to 5.5, 5.6 and 10, respectively), the four Brønsted acid sites detected were constantly located on the same framework oxygen atoms. The first, D1, was on framework oxygen O10 and headed towards the center of the 12-ring; the second, D2, was on the framework oxygen O6 and headed towards the side pocket; the third, D3, was on O5 and headed towards the center of the 12-ring; the last, D4, was on O9 and headed toward the center of the eight-ring through neutron powder diffraction. Hence, it is reasonable to assume the presence of charge compensator protons in these sites. The comparison of powder patterns before and after gallium exchange shows the occurrence of [*301*] and [*200*] *hkl* reflections at the 33.64 and 18.09 ° 2θ angles, respectively. This testifies the presence of the segregate gallium hydroxide phase arising from the gallium-exchange process (Fig.5). The semi-quantitative analysis reveals the presence of 74 and 26 wt % of mordenite and GaO(OH), respectively.

4.2.3 Ga-FER system

Ferrierite (ideal formula $[Mg^{2+}_2Na^{+}_2]$ $[Al_6Si_{30}O_{72}]\bullet 18H_2O$, framework type FER) is a medium pore pentasil zeolite, characterized by a two dimensional channel system built on the intersection of 10-membered and 8-membered ring (10 and 8MR) channels running parallel to the [*001*] and [*010*] crystallographic directions, respectively. 10MR alternating along the *b* direction with the so-called ferrierite cages, structural units originated by the intersection of 8MR and 6MR channels [32]. In this work, due to the absence of *I*-centering forbidden peaks ($h+k+l=2n+1$ reflections), the Ga-FER crystal structure was refined in the *Immm* space group, starting from the atomic coordinates reported by Dalconi et al. (2003) [41]. From the analysis of the lattice parameters obtained through the Rietveld refinement, not noteworthy differences can be detected between the starting NH4-ferrierite [42] and Ga-exchanged samples. Indeed, it is highlighted a very small reduction of the unit cell volume (NH_4-FER=1978.6(1) $Å^3$, Ga-FER=1977.20(15) $Å^3$) principally attributable to the slight decrease of *a* and *b* parameters, whereas *c* remains almost unchanged (NH4-FER: *a*=18.8477(8) Å, *b*=14.1049(5) Å, *c*=7.4425(2) Å; Ga-FER: *a*=18.8394(10) Å, *b*=14.0885(6) Å, *c*=7.4494(2) Å). On the contrary, the comparison of framework bond distances and angles between them, suggests that the metal-exchange process has led to the incorporation of gallium within tetrahedral sites. After the Ga-exchange, <T-O> distances of the four tetrahedral sites appear homogeneously longer (Ga-FER: <T1-O>=1.651 Å, <T2-O>=1.654 Å, <T3-O>=1.653 Å and <T4-O>=1.635 Å; NH4-FER: <T1-O>=1.607 Å, <T2-O>=1.607 Å, <T3-O>=1.609 Å and <T4-O>=1.607 Å), whereas T-O-T angles result narrower than that of the precursor (Table SI6), thus suggesting the presence of tetrahedral Ga^{+3} cations. Indeed, according to Fricke et al. (2000) [5],

structural modifications strongly depend on the concentration of gallium and on the degree of substitution achieved. The analysis of the difference Fourier maps reveals the presence of five partially occupied extraframework sites: three of them are occupied by water molecules (sites labelled W1, W2 and W3), the remaining by gallium cations (sites labelled Ga1 and Ga2). W1, W2 and Ga1 are located within the 10-membered ring, whereas W3 and Ga2 close to the edges of the 8-membered ring window, which defines the limits of the ferrierite cage (Fig.6). As already observed in Ga-L system, no evidences of ammonium are highlighted by the DF analysis, thus indicating that all the NH_4 content has been replaced by gallium after the exchange. Along with the ~ 5 water molecules per unit cell, the refinement of the extraframework Ga^{+3} occupancies highlighted the presence of 1.3 ions per unit cell, in good agreement with the amount of ammonium calculated in the precursor sample (~1.2 ions per unit cell; [42]). The analysis of the extraframework bond lengths reveals the existence of strong interactions among water molecules and Ga^{+3} cations. Distances refined indicate that Ga1 site is four-fold coordinated exclusively to water molecules (Ga1-W1=2.09 Å [x2] and Ga1-W2=2.09 Å [x2]). Besides, W1 and W2 interact between them thus creating W1-W2-W1 short oligomers (W1-W2=2.96 Å [x2], oriented parallel to the 10MR channel which are hydrogen bonded to the O8 framework oxygen atom (O8-W1= 2.53 Å [x4]). Ga2 site is coordinated by the W3 site, as testified by the Ga2-W3=2.06 Å [x2] distance. No other interactions between Ga2 and H_2O were detected and no additional reasonable electronic density residues to be attributed to water were recognized. Considering that, the four-fold coordination is the lowest for Ga^{+3} cations, the presence of some not detectable protons which complete the gallium coordination has to be assumed [43]. Also in this case, the segregate phase of gallium hydroxide was recognized through the qualitative analysis. It has been highlighted by the occurrence of two extra reflections (*i.e.*, [*101*] and [*301*] *hkl* at the 21.41 and 33.61° 2θ angles, respectively) not attributable to the ferrierite and not present in the NH4-FER powder pattern (Fig.7). The semi-quantitative analysis reveals 96 and 4 wt % of ferrierite and GaO(OH), respectively.

4.3 XAS

Fig.8 shows the normalized spectra of all samples and $Ga(NO_3)_3 \bullet xH_2O$ whereas the corresponding $k^2\chi(k)$ experimental data are reported in Fig. 9. As can be seen in the zoom area of Fig. 8, the two peaks in the white line of Ga-exchanged zeolites (at energies of 10375 and 10379 eV) are a preliminary indication of the fact that Ga is present in both tetrahedral and octahedral geometry, according to previous studies [44 45]. The presence of Ga atoms in non-equivalent crystallographic sites, due to the symmetry of the zeolites, together with the secondary phase GaO(OH) in various amount in all the samples (as evidenced by the XRPD data) complicated the EXAFS refinements, so we focused only on the first shell. First-shell contribution has been modelled using Ga–O bond

distances coming from the Ga in tetrahedral sites of the zeolite (as the Ga atoms in extraframework sites have longer bond distances) and the octahedral Ga in GaO(OH) impurity (structural model taken from [46]).

This strategy has been adopted as Ga-O bond distances in tetrahedral and octahedral coordination are quite similar and partially overlapping [47], confirmed also by our quantitative EXAFS results on the first-shell, summarized in Table 3 (fits are shown in Fig. 10 a, b and c).

The obtained average bond lengths are of 1.928 ±0.01 A˚, 1.937 ±0.02 A˚, 1.925 ±0.02 A˚ for Ga-Ferr, Ga-Mor and Ga-L respectively; the refined value (1.04) of the amplitude factor S_0^2 on the $Ga(NO_3)_3 \bullet xH_2O$ reference compound is almost identical to that obtained for the zeolite samples.

As can be seen in Table 3, the major contribution to the EXAFS signal is due to Ga in GaO(OH) impurity, being about 80% in all the samples; nevertheless, a good fit cannot be achieved without introducing also tetrahedral Ga contribution. This fact, together with the XANES information of the splitted peak of the white line (zoom area in Fig. 8), allows us to confirm the presence of tetrahedral Ga and consequent incorporation into the zeolite framework.

CONCLUSIONS

In this work the investigation of the structural features of Gallium substituted L, mordenite and ferrierite zeolites allowed us to elucidate the nature of the gallium active sites combining X-ray powder diffraction (XRPD), X-ray absorption spectroscopy (XAS) and adsorption study. Rietveld structure refinements allowed us to locate and quantify Ga^{+3} cations in framework and non-framework positions as well as determine the presence of water molecules completing the extraframework Ga^{+3} coordination. The lightening of tetrahedral bond distances and narrowing of intertetrahedral angles suggest that the metal cation was incorporated in tetrahedral sites. This is corroborated by XAS analysis, which shows that the average bond lengths derived from the analysis of the first-shell are longer than the <T-O> distances expected in presence of $Si^{4+}$and Al^{3+} as framework cations. All these information are essential not only for their characterization but also for their industrial applications.

ACKNOWLEDGEMENTS.

This study was carried out within a project founded by the “SoWaZe” and grant agreement n° 2017Y2PAB8_003 PRIN program of the Italian Ministry for University and Research (MIUR). We acknowledge Dr. Giuliana Aquilanti (Elettra, Trieste) for the precious suggestions.

REFERENCES

[1] R. Szostak, Handbook of Molecular Sieves, Van Nostrand Reinhold, New York, 1992.

[2] R. Guzzinati, E. Sarti, M. Catani, V. Costa, A. Pagnoni, A. Martucci, E. Rodeghero, D. Capitani, M. Pietrantonio, A. Cavazzini, L. Pasti, ChemPhysChem 19(17) (2018) 2208-2217.

[3] A. Ausavasukhi, T. Sooknoi and D.E. Resasco, J. Catal. 268(1) (2009) 68-78.

[4] V. Kanazirev, V. Mavrodinova, L. Kosova, G.L. Price, Catal. Lett. 9(1-2) (1991) 35-42.

[5] R. Fricke, H. Kosslick, G. Lischke and M. Richter, Chem. Rev. 100(6) (2000), 2303-2406.

[6] A. Bhan and W. Nicholas Delgass, Catal. Rev. 50(1) (2008) 19-151.

[7] K. Yogo, S. Tanaka, M. Ihara, T. Hishiki, E. Kikuchi, Chem. Lett. 21(6) (1992) 1025-1028.

[8] M. Shamzhy, M. Opanasenko, P. Concepción, A. Martínez, Chem. Soc. Rev. 48 (2019) 1095-1149

[9] E.A. Uslamin, B. Luna-Murillo, N. Kosinov, P.C. Bruijnincx, E.A. Pidko, B.M. Weckhuysen, E. J.M. Hensen, Chem. Eng. Sci. 198 (2019) 305-316.

[10] V.B. Kazansky, I.R. Subbotina, R.A. Van Santen and E.J.M. Hensen, J. Catal. 233(2) (2005) 351-358.

[11] R. Szostak, V. Nair, D.K. Simmons, T.L. Thomas, R. Kuvadia, B. Dunson and D.C. Shieh, Stud. Surf. Sci. Catal. 37 (1988) 403-411.

[12] C. Otero Arean, G. Turnes Palomino, F. Geobaldo and A. Zecchina, J. Phys. Chem. 100(16) (1996) 6678- 6690.

[13] C.R. Bayense, A.P. Kentgens, J.W. De Haan, L.J. Van de Ven, and J. H. Van Hooff, J. Phys. Chem. 96(2) (1992) 775-782.

[14] C. Lamberti, G. Turnes Palomino, S. Bordiga, D. Arduino, A. Zecchina and G. Vlaic, Jpn. J. Appl. Phys. 38(S1) (1999) 55-58.

[15] V.D.O. Rodrigues and A.C.F. Júnior, Appl. Catal. A-Gen. 435 (2012) 68-77.

[16] A.I. Serykh, and M.D. Amiridis, Surf. Sci. 603(13) (2009) 2037-2041.

[17] E.A. Pidko and R.A. van Santen, J Phys. Chem. C 113(11) (2009) 4246-4249.

[18] G. Berlier, G. Spoto, P. Fisicaro, S. Bordiga, A. Zecchina, E. Giamello, C. Lamberti, Microchem. J. 71(2-3) (2002) 101-116.

[19] G. Berlier, G. Spoto, S. Bordiga, G. Ricchiardi, P. Fisicaro, A. Zecchina, I. Rossetti, E. Selli, L. Forni, E. Giamello, C. Lamberti, J. Catal. 208(1) (2002), 64-82.

[20] K. Sun, H Xia, E.J.M. Hensen, R.A. van Santen and C. Li, J. Catal. 238(1) (2006) 186-195.

[21] N. Rane, A.R. Overweg, V.B. Kazansky, R.A. Van Santen and E.J.M. Hensen, J. Catal. 239(2) (2006) 478-485.

[22] E.A. Pidko, V.B. Kazansky, E.J.M. Hensen and R.A. van Santen, J. Catal. 240(1) (2006) 73-84.

[23] A. Ausavasukhi and T. Sooknoi, Appl. Catal. A-Gen. 361(1-2) (2009) 93-98.

[24] J. Přech, P. Pizarro, D. P. Serrano and J. Čejka, Chem. Soc. Rev. 47 (2018) 8263-8306.

[25] A.C. Larson, General structure analysis system (GSAS), Los Alamos Nat. Lab.Rep. LAUR (2000) 86–748.

[26] B.H. Toby, J. Appl. Cryst. 34 (2001) 210–213.

[27] A. Di Cicco, G. Aquilanti, M. Minicucci, E. Principi, N. Novello, A. Cognigni and L. Olivi, J. Phys. Conf. Ser. 190(1) 2009 012043.

[28] B. Ravel, M. Newville, J. Synchrotron Rad. 12 (2005) 537–541.

[29] M. Newville, IFEFFIT: interactive XAFS analysis and FEFF fitting, J. Synchrotron Rad. 8 (2001) 322–324.

[30] A. Petushkov, J. Freeman and S.C. Larsen, Langmuir 26(9) (2010) 6695-6701.

[31] M. Ardit, A. Martucci, L. Pasti, E. Rodeghero, G. Beltrami, G. Cruciani, J. Phys. Chem. C. 122(13) (2018) 7249-7259.

[32] C. Baerlocher, L.B. McCusker and D.H. Olson, Atlas of Zeolite Framework Types, 6th rev. ed., Elsevier, Amsterdam, 2007.

[33] R.M. Barrer and H. Villiger, Z. Krist - Cryst Mater. 128(1-6) (1969) 352-370.

[34] J. M. Newsam, J. Chem. Soc, Chem. Commun. 2 (1987) 123-124.

[35] E. Stuckenschmidt, W. Joswig, W.H. Baur, Eur. J. Mineral. 8 (1996) 85-92.

[36] E. Cannillo, A. Coda, G. Fagnani, Acta Cryst. 20(2) (1966) 301-309.

[37] A. Sani, G. Cruciani, Phys. Chem. Miner. 29(5) (2002) 351-361.

[38] G. Cruciani, A. Martucci and C. Meneghini, Eur. J. Mineral. 15(2) (2003) 257-266.

[39] A. Alberti, P. Davoli, and G. Vezzalini, Z. Krist - Cryst Mater. 175(1-4) (1986) 249-256.

[40] A. Martucci, G. Cruciani, A. Alberti, C. Ritter, P. Ciambelli, and M. Rapacciuolo, Micropor. Mesopor. Mat. 35 (2000) 405-412.

[41] M.C. Dalconi, A. Alberti, G. Cruciani, P. Ciambelli and E. Fonda, Micropor. Mesopor. Mat. 62(3) (2003) 191-200.

[42] A. Martucci, L. Leardini, M. Nassi, E. Sarti, R. Bagatin, and L. Pasti, Mineral. Mag. 78(5) (2014) 1161-1176.

[43] Y.V. Joshi and K.T. Thomson, Catal. Today 105(1) (2005) 106-121.

[44] K. Nishi, K. Shimizu, M. Takamatsu, H. Yoshida, A. Satsuma, T. Tanaka, S. Yoshida, T. Hattori, J. Phys. Chem. B 102(50) (1998) 10190-10195.

[45] M. Akatsuka, T. Yoshida, N. Yamamoto, M. Yamamoto, S. Ogawa and S. Yagi, J. Phys. Conf. Ser. 712(1) 2016 012056.

[46] S.J. Li, C. Zheng, and K.C. Lobringn, Z. Krist -New Cryst. St. 218(JG) (2003) 11-12.

[47] O. C. Gagné and F.C. Hawthorne, Acta Crystallogr. B 74(1) (2018) 63-78.

[48] A.D. Hendsbee, C.C. Pye and J.D. Masuda, Acta Crystallogr. E65(8) (2009) i65-i65.

Figures

Figure 1. Adsorption of gallium on a) L zeolite, b) Ferrierite and c) Mordenite.

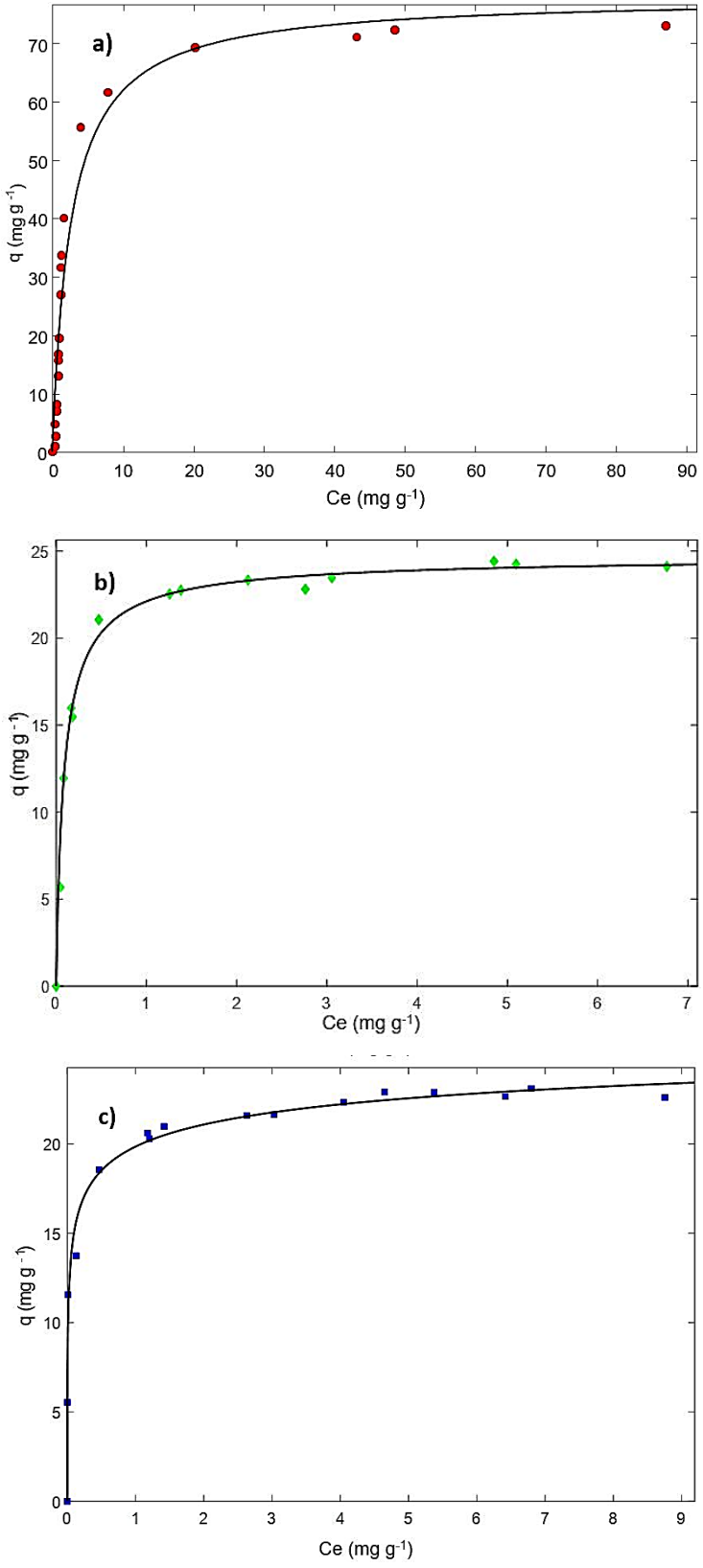

Figure 2. Extraframework content distribution of Ga-L system. Projection along *c* (a) and *a* (b)

axis.

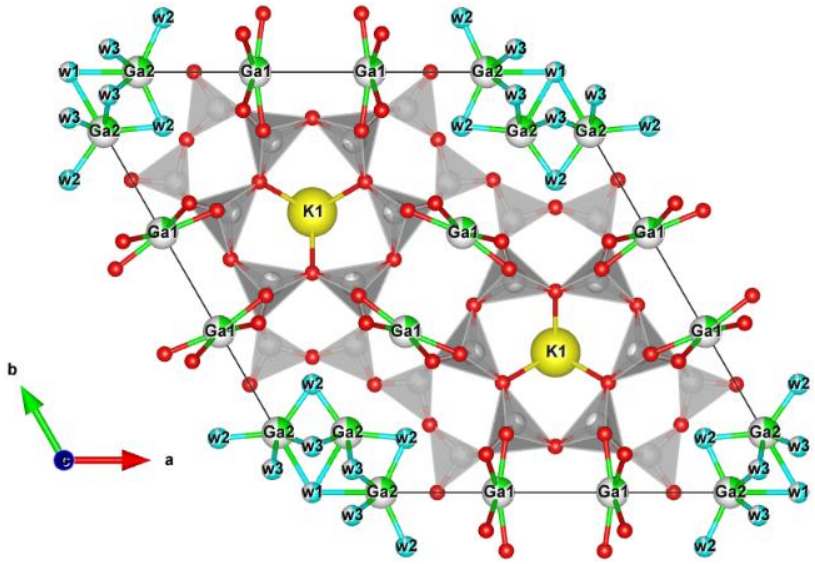

a)

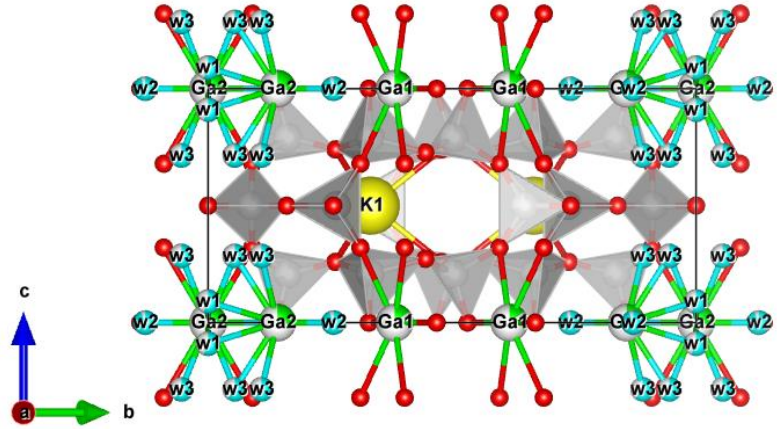

b)

Figure 3. Powder diffraction pattern of Ga-L system.

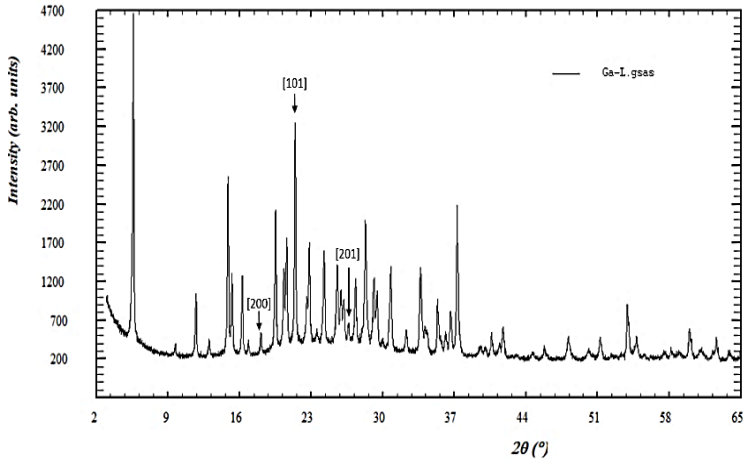

Figure 4. Extraframework content distribution of Ga-MOR system. Projection along *c* (a) and *a* (b)

axis.

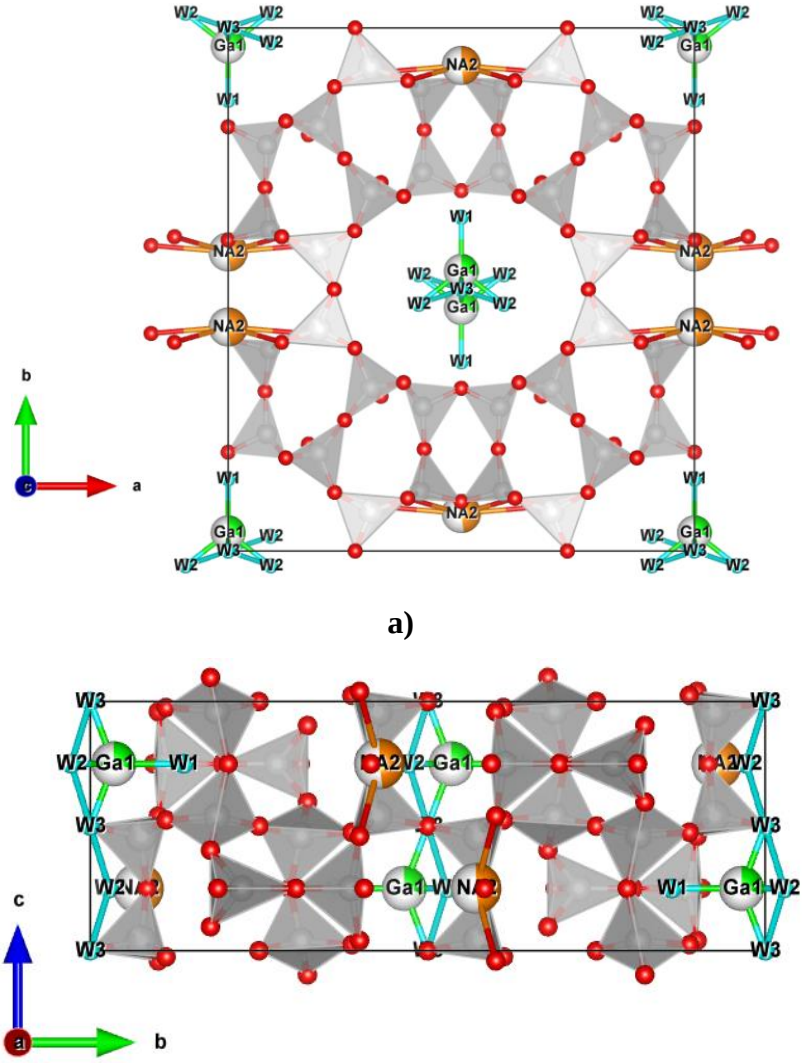

a)

b)

Figure 5. Powder pattern of Ga-MOR system.

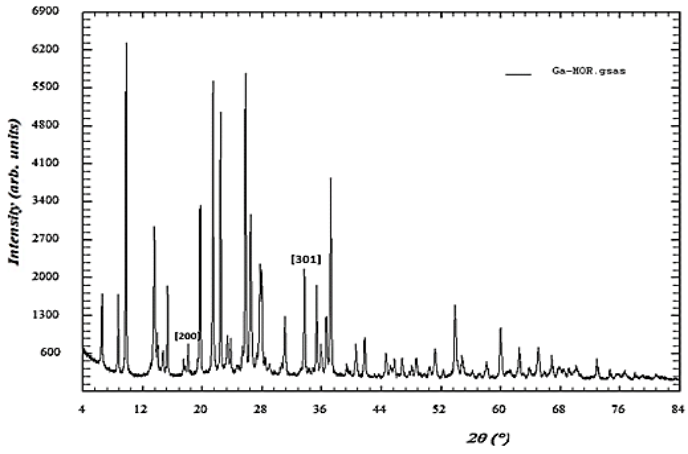

Figure 6. Extraframework content distribution of Ga-FER system: projection along *c* (a) and *a* (b)

axis.

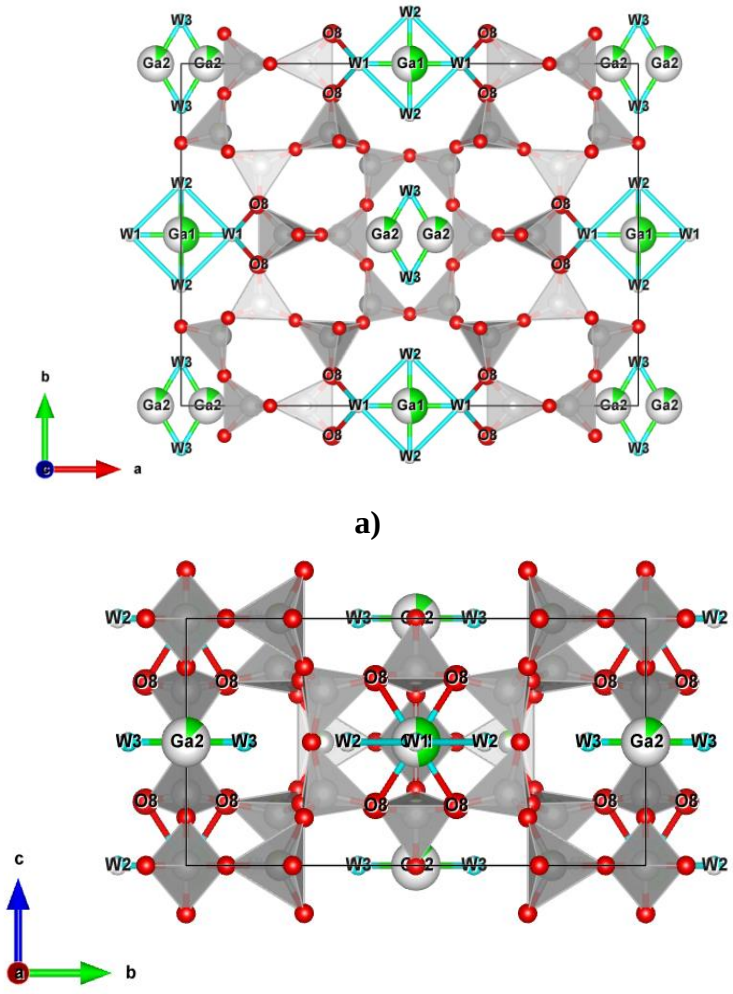

Figure 7. Powder pattern of Ga-FER system.

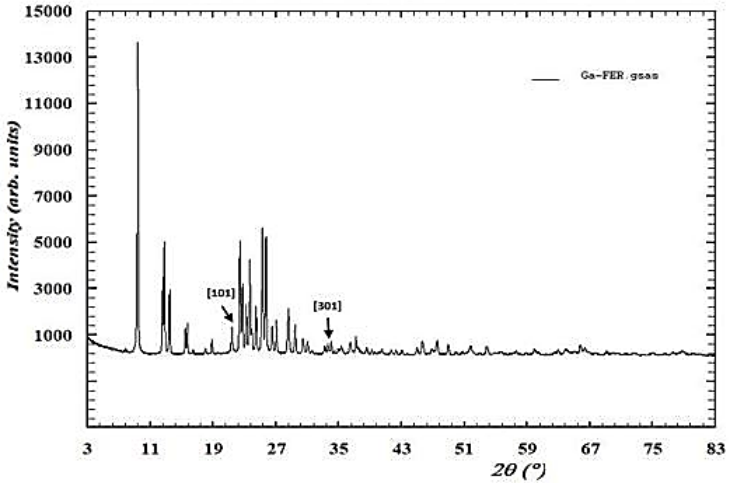

Figure 8. Normalized spectra of Ga-MOR (green), Ga-FER (blue), Ga-L (red) and $Ga(NO_3)_3$ reference (grey). Small box on the top right is a zoom around the edge area.

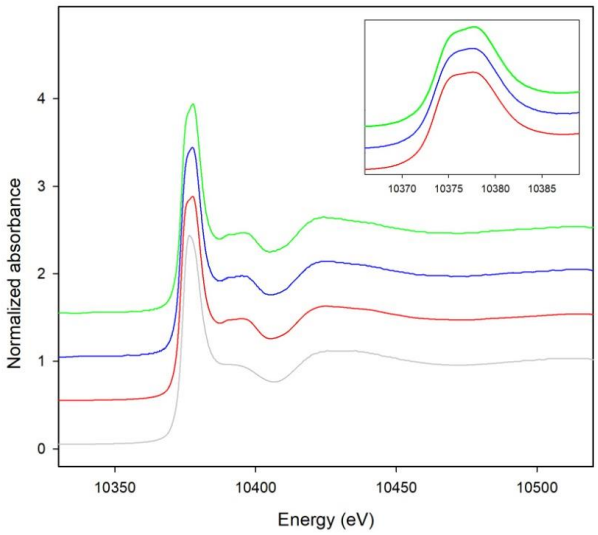

Figure 9. kχ(k2) experimental data of Ga-MOR (green), Ga-FER (blue) and Ga-L (red).

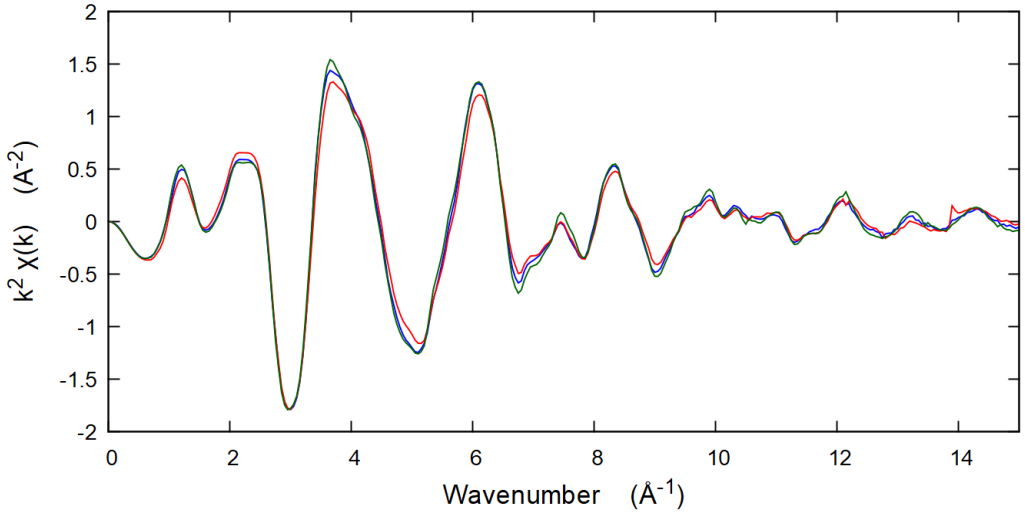

Figure 10. The obtained EXAFS fit on the three samples: a) Ga-FER; b) Ga-MOR; c) Ga-L.

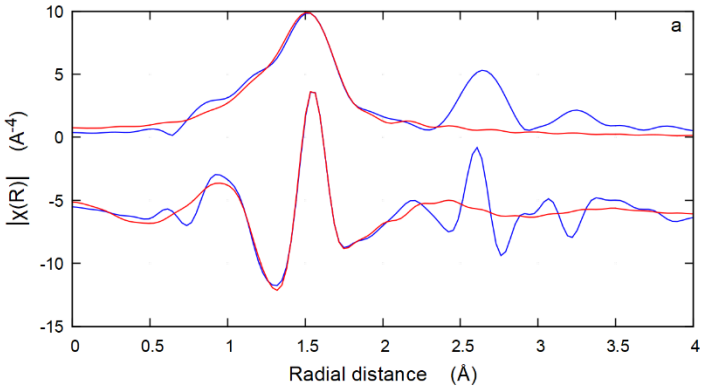

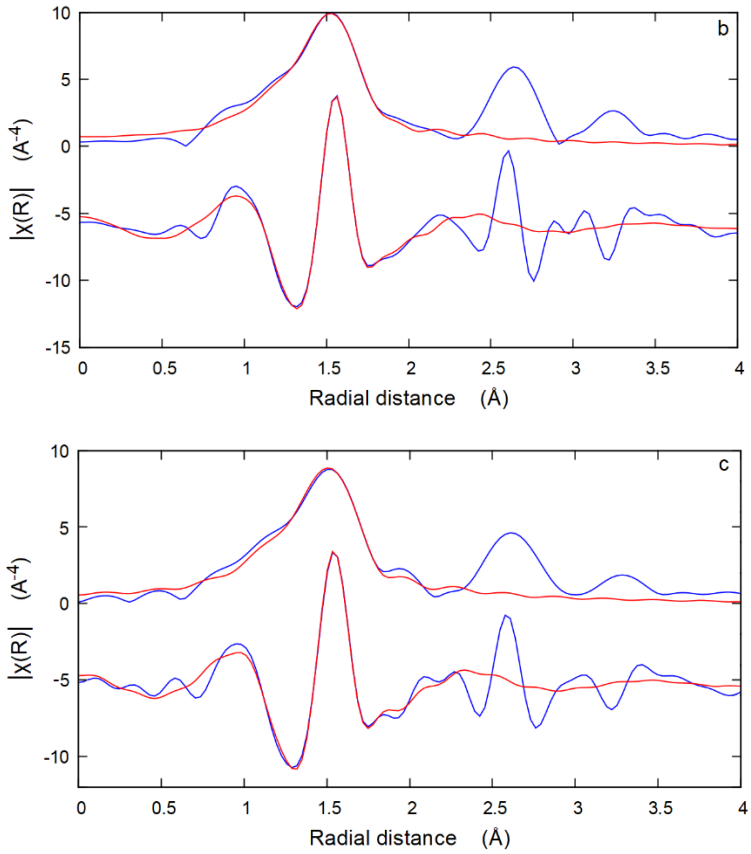

Tables

Table 1
Crystallographic data obtained from the Rietveld refinements of Ga-L, Ga-MOR and Ga-FER systems.

Parameter	Ga-L	Ga-MOR	Ga-FER
	$Ga_{2.57}K_2((GaAlSi)_{36}O_{72}) \cdot 14H_2O$	$Ga_{1.16}Na_2((GaAlSi)_{48}O_{96}) \cdot 13H_2O$	$Ga_{1.3}((GaAlSI)_{36}O_{72}) \cdot 5H_2O$
Wavelength (Å)	1.54059	1.54059	1.54059
2θ (°) range	5.5-100	5.5-100	5.5-100
N_{obs}	1339	1482	1564
N_{var}	56	76	64
R_{wp} (%)	14.45	13.35	14.59
R_p (%)	10.83	10.17	11.34
R_F^2 (%)	16.85	11.32	12.29

$$R_p = \sum[Y_{io} - Y_{ic}]/\sum Y_{io} \; ; \; R_{wp} = [\sum wi(Y_{io} - Y_{ic})^2/\sum wi Y_{io}^2]^{0.5} \; ; \; R_F^2 = \sum |F_o^2 - F_c^2|/|F_o^2|$$

Table 2
Gallium cation exchange isotherm parameters. q_e (mg g^{-1}): exchanged concentration at equilibrium; C_e (mg dm^{-3}): concentration in the solution at equilibrium; K_L, K_T (dm^3 mg^{-1}): affinity constants for the Langmuir and the Tóth models, respectively; q_s (mg g^{-1}) cation exchange capacity; v heterogeneity parameter in the Tóth model (see text for further details). Confidence bounds at 95% of probability are reported in parenthesis.

Parameters	L	FER	MOR
q_s (mg g^{-1})	78.02 (70.71, 85.33)	24.52 (23.86, 25.17)	21.36 (20.07, 22.65)
K_L (dm^3 mg^{-1})	0.3841 (0.2723, 0.4959)	9.946	34.9 (17.87, 51.9)

		(8.329, 11.56)	
R^2	0.9505	0.9913	0.9328
q_s (mg g^{-1})	71.16 (65.61, 76.71)	24.76 (23.72, 25.8)	30.47 (21.88, 39.07)
K_T (dm^3 mg^{-1})	0.2788 (0.2191, 0.3385)	14.14 (7.92, 20.36)	38.4 (25.7 52.3)
v	0.83 (0.42, 1.24)	0.86 (0.64, 1.08)	0.2291 (0.1135, 0.3447)
R^2	0.9696	0.9954	0.9874

Table 3
Crystallographic data and structural parameters as obtained from the R-space fit by using the theoretical references.

Sample	Shells	%	Ref.	N	R(Å)[a]	S_0^2	R-factor	σ^2(Å^2)	ΔE_0(eV)
$Ga(NO_3)_3 \bullet xH_2O$			[48]			1.04 (8)	0.012	0.007 (1)	6 (1)
	Site1 - Ga – O_1	0.5		6	1.939 (4)				
	Site2 - Ga – O_4	0.5		4	1.935 (4)				
	Site2 - Ga – O_5			2	1.961 (4)				
Fer						1.05 (5)	0.003	0.002 (2)	2 (2)
	Site1[b] - Ga – O	0.2 (1)*0.5		4	1.93 (1)				
	Site2[b] - Ga – O	0.2 (1)*0.5		3	1.91 (1)				
	Site2[b] - Ga – O			1	1.94 (1)				
	GaO(OH) contamination:		[46]					0.005 (1)	
	Ga – O_1	0.8 (1)		3	1.904 (6)				
	Ga – O_2			3	2.031 (6)				
Mor						1.05 (4)	0.003	0.001 (3)	3 (1)
	Site1[b] - Ga – O	0.15 (8)*0.5		4	1.96 (2)				
	Site2[b] - Ga – O	0.15 (8)*0.5		4	1.92 (2)				
	GaO(OH) contamination:		[46]					0.005 (2)	
	Ga – O_1	0.85 (8)		3	1.912 (8)				
	Ga – O_2			3	2.040 (8)				
L						1.05 (9)	0.004	0.001 (3)	3 (1)
	T1 - Ga – O_4	0.16 (4)*0.5		4	1.93 (2)				
	T2 - Ga – O_5	0.16 (4)*0.5		2	1.91 (2)				
	T2 - Ga – O_6			2	1.94 (2)				
	GaO(OH) contamination:		[46]					0.007 (2)	
	Ga – O_1	0.84 (4)		3	1.900 (3)				
	Ga – O_2			3	2.026 (3)				

[a]All the bond lengths values are in excellent agreement with the mean values reported by Gagné and Hawthorne (2018) [47] for Ga^{+3} ion in both tetrahedral and octahedral coordination.
[b]These sites represent an average of the Ga atoms in tetrahedral coordination and did not refer to the real crystallographic sites.